Hypertension Research (2015) 38, 723–732

www.nature.com/hr

ORIGINAL ARTICLE

Chronic arterial hypertension impedes glioma growth: a multiparametric MRI study in the rat

Annelise Letourneur[1,2,3,4], Simon Roussel[1,2,3,4], Myriam Bernaudin[1,2,3,4], Fabien Fillesoye[1,2,3,4], Jérôme Toutain[1,2,3,4], Eric T MacKenzie[1,2,3,4], Edwige Petit[1,2,3,4], Omar Touzani[1,2,3,4] and Samuel Valable[1,2,3,4]

Glioblastoma is the most aggressive brain tumor and is almost always fatal. These tumors are highly vascularized and angiogenesis is one of the pre-eminent mechanisms underlying their growth. Chronic arterial hypertension (CAH) is a common and worldwide pathology that markedlly alters the structure and function of the vasculature. Yet, essential hypertension is associated in the brain with potential locally impaired vasoreactivity, disturbed perfusion supply and hypoxia phenomena. Even though CAH is a global burden and has an important impact on brain function, nothing is known about the way this frequent pathology would interact with the evolution of glioma. We sought to determine if arterial hypertension influences gliobastoma growth. In the present study, rat glioma C6 tumor cells were implanted in the caudate–putamen of spontaneously hypertensive rats (SHR) or their normotensive controls, the Wistar–Kyoto (WKY) rats. The evolution of the tumor was sequentially analyzed by multiparametric magnetic resonance imaging and the inflammatory response was examined by histochemistry. We found that CAH significantly attenuates the growth of the tumor as, at 21 days, the volume of the tumor was 85.4 ± 34.7 and $126.1 \pm 28.8\,mm^3$, respectively, in hypertensive and normotensive rats ($P<0.02$). Moreover, cerebral blood volume and cerebral blood flow were greater in the tumors of hypertensive rats ($P<0.05$). The lesser growth of the tumor observed in normotensive animals was not due to an enhanced rejection of the tumor cells in WKY rats, the inflammatory response being similar in both groups. For the first time, these results show that CAH impedes the growth of glioblastoma and illustrate the need to further study the impact of hypertension on the evolution of brain tumors.
Hypertension Research (2015) **38,** 723–732; doi:10.1038/hr.2015.66; published online 18 June 2015

Keywords: brain tumor; chronic arterial hypertension; glioma; glioblastoma; MRI; rat

INTRODUCTION

Glioblastoma (GBM) or grade IV astrocytoma is the most vigorous and malignant primary brain tumor, which is rapidly fatal.[1,2] These tumors are highly vascularized and it is acknowledged that angiogenesis is one of the predominant features that regulate glioma growth.[3,4] Repressing angiogenesis is a promising therapeutic strategy for these tumors.[5,6]

Chronic arterial hypertension (CAH) is a major public health problem as >25% of the adult worldwide population is hypertensive and its incidence is still increasing.[7] Although antihypertensive treatments are widely available, adequate control of hypertension is ineffectively achieved in the adult population,[8,9] whereas, especially in the elderly, it would be highly beneficial[10] as CAH is associated with other cardiovascular pathologies and vascular dementia.[11] Moreover, CAH is the principal risk factor for vascular pathologies such as stroke and ischemic heart diseases.[12] These latter disease states are mainly attributable to CAH-induced alterations of the vasculature. Indeed, in the brain as well as in the periphery, elevated arterial pressure (AP) results in structural and functional vascular changes such as hypertrophy or remodeling of the microcirculation with vessel rarefaction.[13,14] Within the cerebral circulation, CAH impairs the phenomenon of autoregulation, resulting in a shift of the curve to higher values of perfusion pressure.[15] CAH induces structural vascular changes leading to angiopathy, and also leads to dynamic vascular changes. Among functional disturbances, a widespread cerebral blood flow decrease is observed as being the most severe in the hippocampus and several cortical areas.[16] Owing to those modifications, CAH induces microaneurysms and microhemorrhages, as well as related cognitive impairment.[17] Patients suffering from CAH also exhibit white matter damage caused by neuropathological processes, including not only vascular impairment, as described previously, but also inflammation and blood–brain barrier breakdown. Under CAH, the brain parenchyma suffers from vascular and cellular inflammation, endothelial dysfunction and free radical generation.[18,19]

[1]CNRS, UMR 6301 ISTCT, CEA, Université de Caen Basse-Normandie 'Imaging and Therapeutical Strategies in Cerebral and Tumoral Pathologies'; CERVOxy team, GIP 'Hypoxia, Cerebrovascular and Tumoral Pathophysiologies' CYCERON, Caen, France; [2]CEA, DSV/I2BM, UMR 6301 ISTCT, Caen, France; [3]Université de Caen Basse-Normandie, Caen, France and [4]Normandie Univ, Caen, France
Correspondence: Dr A Letourneur, CNRS, UMR 6301 ISTCT, CEA, Université de Caen Basse-Norma ndie 'Imaging and Therapeutical Strategies in Cerebral and Tumoral Pathologies'; CERVOxy team, 'Hypoxia, Cerebrovascular and Tumoral Pathophysiologies' CYCERON, Bd Henri Becquerel, Caen 5229, France.
E-mail: letourneur@cyceron.fr
Received 10 November 2014; revised 20 January 2015; accepted 16 April 2015; published online 18 June 2015

On the other hand, angiogenesis has also been reported to be influenced by CAH. Indeed, rarefaction of the small arteries and a decrease in the density of the capillaries have been shown in animal models of hypertension,[20] as well as in patients.[21–23] Interestingly, antihypertensive treatments can restore altered angiogenesis.[20,24] Although angiogenesis is altered by CAH, angiotensin, which is one of the main promoters of angiogenesis, increased during HTA (especially in certain types of HTA). The hypoxic state created by the decreased cerebral blood flow (CBF), stroke, microaneurysms and microbleedings, as well as the inflammatory character of the pathology, would be more favorable for tumor growth.

Given the effects of CAH on the vasculature and the contribution of neovascularization in tumor growth, here we ask a specific question: does CAH enhance the growth of an aggressive glioma? Our hypothesis was that CAH-induced alterations in the cerebral microcirculation would influence tumor growth. To test this hypothesis, we have implanted tumor cells of the C6 line into the caudate–putamen (CPu) of spontaneously hypertensive rats (SHR) or their normotensive controls, the Wistar–Kyoto (WKY) rats. The SHR is considered to be a model of essential hypertension, and this strain is the most widely used in the studies of the pathophysiology and treatment of hypertension.[25] The C6 glioma is remarkably similar to human GBM with respect to vascularization, morphology, necrosis and hypoxia.[26–28] The growth of the tumor and its hemodynamic status were studied by sequential multiparametric magnetic resonance imaging (MRI) and inflammation was analyzed by histochemistry.

METHODS

Animals

Male SHR ($n=9$; 296 ± 36 g) and WKY ($n=9$; 322 ± 19 g) rats at the time of entry into the study were purchased from the JANVIER breeding center (Centre d'Elevage René Janvier, Le Genest-St-Isle, France). All animal experiments were carried out under the previous European directive (86/609/EEC) as enacted in the national legislation. Individual licenses to investigate SR (14–26), MB (14–71), JT (14–45), EP (14–79), OT (14–29) and SV (14–55) are held and the study was approved by the regional ethical committee for animal research and health-care 'Comité Régional d'Éthique en matière d'Expérimentation Animale pour la Normandie' (CEEAN, agreement no. 0507-02). Rats, fed with standard laboratory chow and receiving water *ad libitum*, were housed in animal care facilities (Centre Universitaire de Ressources Biologiques (CURB), approval no. B14118015) immediately adjacent to the complex of experimental and imaging laboratories (GIP-Cyceron, approval no. B14118001). During all the experiments, the body weights of the rats were measured daily and the general status of the animals was carefully followed. There was no mortality before the experimental end of the protocol; however, one WKY rat was excluded because of postimplantation technical failure. All the experiments were performed randomly and in a blinded manner.

AP measurements in awake rats

AP was measured through the use of the tail cuff method (Storage pressure meter-5002; Letica, Barcelona, Spain).[29] AP measurements were performed 1 month and 2 weeks before the implantation of C6 cells. To ensure correct AP assessments, rats were prewarmed (35 °C) and measures were repeated five times for each session.

Glioma model

The C6 glioma (ATCC, Manassas, VA, USA; CCL-107) was chosen as the tumor model.[27,30] C6 glioma cells (ATCC, CCL-107; cell passage 20) were cultured for 3 days in DMEM containing $1\,g\,l^{-1}$ glucose supplemented with 10% bovine fetal serum, 2 mM glutamine and 1% penicillin–streptomycin, and then trypsinized to obtain the cell suspension for implantation. SHR and WKY rats were anesthetized with isoflurane (2%) in a mixture of 30% O_2 and 70% N_2O. The body temperature was maintained around 37.5 °C with a feedback-controlled heating pad (Homeothermic Blanket Harvard, Holliston, MA, USA) connected to a rectal probe. Rats were placed in a stereotaxic head holder (David Kopf Instruments, Elmo St Tujunga, CA, USA), and then a midline scalp incision was performed and the calvarium was exposed. The skull was drilled with a saline-cooled dental burr to produce a 1 mm hole allowing the insertion of a dental needle, which was left in place for 3 min before injection. The cell suspension (1×10^5 cells in 3 µl phosphate-buffered saline) was injected into the right CPu (coordinates relative to bregma: 3.0 mm lateral and 6.0 mm deep) according to the rat stereotaxic atlas (Paxinos and Watson, 2006)[31] at a constant flow of $0.3\,\mu l\,min^{-1}$ over 10 min. The needle was left in place 5 min after the end of the injection and then slowly removed. The scalp was sutured and the rats were allowed to recover from anesthesia.

MRI examinations

MRI examinations were performed on a 7-T horizontal Bruker magnet (Pharmascan, Ettlingen, Germany). Rats were anesthetized with 2% isoflurane and placed into a head holder within the magnet. Body temperature and respiratory rate were monitored throughout the MRI scans. MRI sessions were performed at days (D) 11, 18 and 21 after cell implantation. Ten contiguous slices of 1.5 mm thick were acquired for diffusion-weighted imaging, fast T2 and fast T1, and a 38.4x38.4 mm^2 field of view was used (except for echo-planar imaging T2* and fast low-angle shot T2*). Diffusion-weighted imaging was acquired with the following parameters: 1-shot spin echo echo-planar images, 80x80 matrix, $0.480\times0.480\,mm^2$ resolution, TR/TE (echo time and repetition time) = 3500/34.95 ms, *b*-values = 0, 500 and $1000\,s\,mm^{-2}$ and 3 directions. Apparent diffusion coefficient (ADC) maps were then calculated. Fast T2 (rapid acquisition with refocused echo factor 8) was also acquired at the three time points with the following parameters: 256x192 matrix, $0.150\times0.200\,mm^2$ resolution and TR/TE = 5000/74 ms. Perfusion-weighted imaging was performed at D11 and D18 after an intravenous bolus injection of a contrast agent ($0.3\,mg\,kg^{-1}$, gadopentetate dimeglumine diethylenetriaminepentaacetic acid (Gd-DTPA); Magnevist Bayer Schering Pharma AG, Leverkusen, Germany) and dynamic susceptibility contrast MRI. T1-enhanced imaging was acquired 2 min after each echo-planar imaging T2* with a fast T1 sequence (rapid acquisition with refocused echo factor 4), 256×256 matrix, $0.150\times0.150\,mm^2$ resolution and TR/TE = 1300/7.334 ms.

Immunohistochemistry

Immediately after the last MRI session (i.e. at D21), the animals were deeply anesthetized and intracardially perfused with a heparinized saline solution followed by paraformaldehyde (4%) in phosphate buffer (pH 7.4). Fixed brains were then cryoprotected by immersion in a 30% sucrose solution during 72 h and cut with a freezing microtome (Microm HM 450; Thermo Scientific, Walldorf, Germany) in 50-µm-thick coronal slices. One slice every 350 µm was collected for thionin staining. The stained sections were then photographed and tumor volumes as well as hemispheric volumes were calculated using the ImageJ software.[32,33] The brain was cut from the rostral to the caudal pole so as to delineate (in a blind manner) the axial extremes of the tumor.

For the other sections, immunolabeling was performed. After saturation in phosphate-buffered saline/0.01% Tween/3% bovine serum albumin for 1 h at room temperature, slices were incubated overnight (4 °C) with specific endothelial cell antibodies: mouse anti RECA-1 (rat endothelial cell antigen-1) (1:100; AbD Serotec, Kidlington, UK.), and visualization was performed using a cyanine 3-linked goat anti-mouse IgG (1:1000; Jackson ImmunoResearch Laboratories, West Grove, PA, USA). Nuclear cells were counterstained with Hoechst 33342 ($1\,\mu g\,ml^{-1}$; Sigma, France) in Dako fluorescent mounting medium (DakoCytomation, Glostrup, Denmark).

Post-mortem vessels morphology analysis

Microvessel density (vascular surface) and size (length and diameter) were analyzed in five regions of interest (ROI): striatal tumor center, cortical tumor center, striatal tumor periphery and cortical and striatal areas in the contralateral hemisphere. The periphery of the tumor has been defined as a 200 µm width band around the tumor center.[34] Images were acquired with a fluorescent microscope (Leica DM 6000, Wetzlar, Germany) equipped with a camera. Analyses were performed using home-made ImageJ macros.[35] Images

($2000 \times 1500\ \mu m^2$) to visualize RECA-1 and Hoechst 33342 were taken at x10 and x40 in each of the five ROIs for at least five slices per animal ($n = 8$ rats per group). Then, the photographs of vessels were binarized by local thresholding at the mean between the minimum and maximum intensity of their neighborhood, thus segmenting vessels at half-height. Vessel density was computed as the surface occupied by vessels; the vessel length was derived from skeletonization. The vessel diameter at each pixel location along the skeletons was determined using distance maps.[35]

Post-mortem analysis of inflammation

Lectin histochemistry for the specific visualization of activated microglia and macrophages was performed. Briefly, after endogenous peroxidase blockade with 3% hydrogen peroxide, free-floating slices were incubated with peroxidase-lectin (peroxidase-linked isolectin B4; isolated from *Griffonia simplicifolia* GS-B4, 1:100; Sigma) in phosphate-buffered saline-Ca^{2+}-Triton (1:200). Following several washes in phosphate-buffered saline-Ca^{2+}, the peroxidase reaction product was revealed with the 3,3'-diaminobenzidine (DAB substrate kit for peroxidase SK4400; Vector Laboratories, Burlingame, CA, USA) with buffer stock solution and hydrogen peroxide in distilled water. Slides were then counterstained with thionin.

MRI data analysis

MR images were analyzed by in-house macros based on the ImageJ software. Tumor volumes were calculated at different time points by the semiautomatic analysis of images. Abnormal signals were defined on all the fast T1-weighted post-Gd and fast T2-weighted slices by thresholding at the mean ± 2 s.d. of the contralateral, healthy tissue values. The cortical and the CPu contribution to the tumor were then manually separated and the volume measured. Assuming an exponential tumor growth, tumor volumes were then expressed by a natural logarithm function. On ADC maps, the tumors were manually delineated. Cerebral blood volume (CBV) and CBF were derived from the analysis of the data derived from the first pass of Gd-DTPA. Briefly, an intra-animal spatial and temporal coregistration was initially performed for each first-pass experiment. Masks of each hemisphere (without ventricles) and masks of the tumor were created. The signal obtained in each ROI was fitted to a gamma-variate function. CBF and CBV in each ROI were then calculated by the DSCoMAN ImageJ plug-in, which implements the Boxerman–Weisskoff algorithm.[35]

Statistical analyses

Data are represented as mean ± s.d. The statistical analyses were performed with analysis of variance (ANOVA) followed, when appropriate, by Tukey's honestly significant difference (HSD), ANOVA one-factor or *t*-test (JMP software, SAS Institute Inc., Cary, NC, USA). We used two-factor repeated-measures ANOVA to analyze the evolution of perfusion-weighted imaging abnormalities and tumor growth.

RESULTS

Body weight and AP

The overall state of the animals was evaluated on a daily basis. The rats presented a constant weight along the experimental time period (Table 1). Their weights at D11, D18 and D21, respectively, after tumor implantation were: 366 ± 35, 367 ± 36 and 370 ± 35 g for WKY ($n = 8$) rats and 301 ± 29, 304 ± 29 and 300 ± 29 g for SHR ($n = 9$) rats. APs in awake SHR were significantly greater than those measured in awake WKY. Systolic (sAP) and diastolic (dAP) AP were, respectively, 206 ± 12 and 160 ± 15 mmHg in SHR and 135 ± 12 and 105 ± 15 mmHg in WKY rats ($P < 0.0001$ for both sAP and dAP) (see Table 1 for more details).

Evolution of tumor growth

In both normotensive and hypertensive rats, the tumors were clearly visible on fast T1- and T2-weighted imaging at D11 after the cell implantation. T1-enhanced imaging and T2 imaging were used to study the tumor volume. For both imaging modalities, we performed a two-factor ANOVA (groups and time points) to demonstrate a significant group effect ($P < 0.05$), time effect ($P < 0.0001$) and a significant interaction group × time ($P < 0.015$ for T1 and $P < 0.003$ for T2 imaging), all of which allow one to evaluate the group effects at the different time points. At D11, there was no significant difference in the tumor volumes between SHR and WKY even if a tendency could be detected (Figures 1a and b).

One week later (D18), the hypertensive rats displayed lesser tumor volumes compared with their normotensive controls. In hypertensive rats, the tumor volumes were statistically less important on enhanced T1-weighted imaging (57.1 ± 22.1 *vs.* 77.6 ± 13.6 mm^3, respectively, for SHR and WKY; $P < 0.04$, *t*-test), whereas T2-weighted imaging failed to reveal a significant difference at D18 (55.1 ± 22.0 *vs.* 67.8 ± 9.8 mm^3, respectively, for SHR and WKY; $P = 0.15$, Tukey's HSD following a significant ANOVA) (Figures 1a and b).

At D21, the tumor was still significantly less expansive in SHR (85.4 ± 34.7 mm^3) relative to WKY rats (126.1 ± 28.8 mm^3) ($P < 0.02$; Tukey's HSD following a significant ANOVA) (Figures 1b). The comparison of the kinetics of the growth of tumors between the two groups confirmed a less rapid development of the tumors for the hypertensive rats in comparison with the normotensive rats ($P < 0.007$, *t*-test for slopes; no significant differences in intercepts; $y = 0.27\ (\pm 0.035)x - 0.79$ for WKY and $y = 0.20\ (\pm 0.050)x + 0.17$ for SHR) (Supplementary Data). As the tumors affected both the cortex and the CPu, we further analyzed tumor growth separately in each region. In hypertensive animals, the cortical portion of the tumor showed a tendency to be less extensive compared with that in normotensive animals, but the major difference was seen with CPu tumor volume (T2-MRI; ANOVA on cortical tumor volume—group effect: $P < 0.35$; time effect: $P < 0.0001$; interaction time × group: $P < 0.15$; Supplementary Data A). The CPu tumor was significantly less extensive in SHR compared with that in WKY ($P = 0.014$, *t*-test

Table 1 Monitoring of cardiovascular parameters before experiment and animal weights along the experiment

	Cardiovascular parameters									*Body weight (g)*				
	D−21→−15			*D−15→−7*			*D−7→0*							
	HR	*sAP*	*dAP*	*HR*	*sAP*	*dAP*	*HR*	*sAP*	*dAP*	*D0*	*D5*	*D11*	*D18*	*D21*
SHR ($n=9$)	407 ± 27	218 ± 13	171 ± 18	436 ± 33	202 ± 24	158 ± 16	444 ± 35	200 ± 9	151 ± 14	296 ± 36	301 ± 29	301 ± 29	305 ± 29	299 ± 29
WKY ($n=8$)	392 ± 44	141 ± 7	110 ± 8	431 ± 48	130 ± 18	97 ± 14	461 ± 12	142 ± 8	107 ± 22	323 ± 20	348 ± 23	367 ± 35	368 ± 36	370 ± 35

Abbreviations: AP, arterial pressure; dAP, diastolic AP; HR, heart rate; sAP, systolic AP; SHR, spontaneously hypertensive; WKY, Wistar–Kyoto.
The AP was monitored once a week before the tumor implantation. The HR was similar and stable in both strains. The AP measurements were stable over the same interval of time and over the different times. SHR displayed at each time point a significantly higher AP, with higher sAP and dAP, compared with WKY rats. Along the experiment, the weight of all the animals was assessed on a daily basis; for clarity, only few time points are indicated in the table. The animals presented a normal and healthy weight following the striatal implantation (D0).

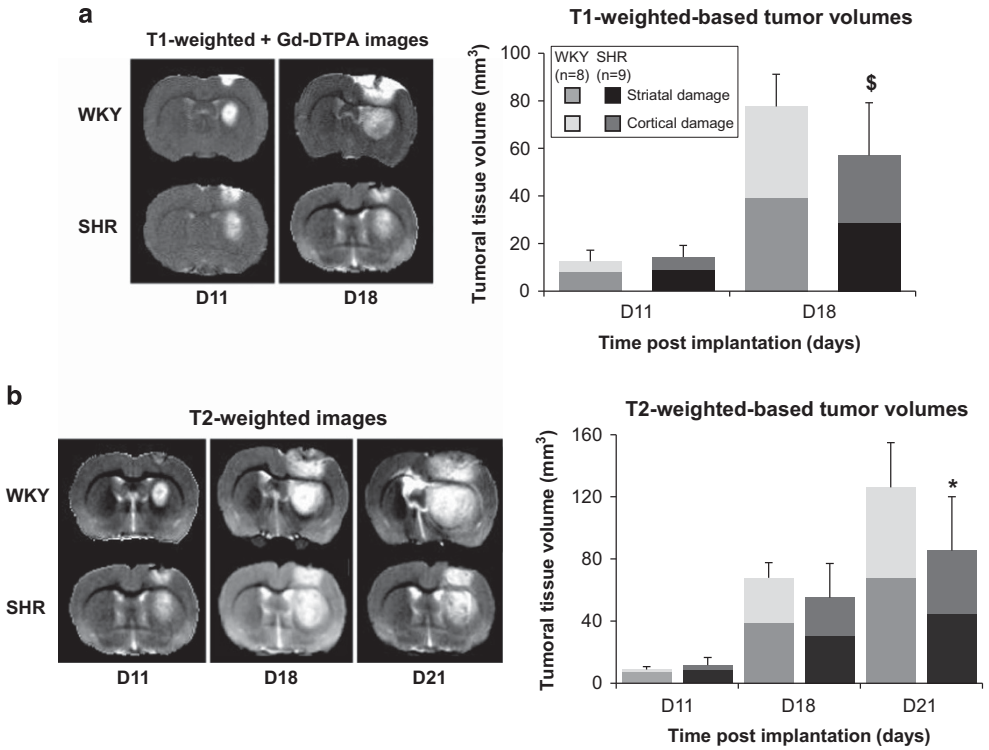

Figure 1 (**a**) Representative fast T1-weighted images acquired at days 11 and 18 after implantation in normotensive (Wistar–Kyoto (WKY)) and hypertensive (spontaneously hypertensive rats (SHR)). There was no difference between SHR and WKY rats in tumor volumes at day 11 after tumor cell implantation. At day 18, the tumoral tissue volume, defined on fast T1-weighted images, was significantly lesser in SHR compared with WKY rats. $One-factor analysis of variance (ANOVA), group effect at day 18 ($P<0.04$) following a two-factor ANOVA showing a significant interaction ($P<0.015$). (**b**) Representative T2-weighted images acquired at days 11, 18 and 21 after implantation revealed that the tumor was less voluminous in hypertensive compared with normotensive rats. The tumor was not markedly different between WKY and SHR at 11 days after implantation, but thereafter the SHR volumes increased less rapidly compared with those of the WKY rats. *One-factor ANOVA, group effect at day 21 ($P<0.0023$) following two-factor ANOVA showing a significant interaction ($P<0.0031$).

at D21 following significant ANOVA (interaction time × group: $P<0.004$); Supplementary Data B). In normotensive rats, we observed a shift of the midline translated by a significant volumetric compression of the healthy hemisphere in normotensive animals compared with hypertensive rats. The degree of midline shift was estimated by the ratio of the volume of the implanted hemisphere divided by the volume of the contralateral, healthy counterpart. In the WKY rats, the ratio (1.24 ± 0.05) was significantly more important ($P<0.001$) compared with that in the SHR (1.16 ± 0.08), in which the value was closer to unity. All implanted rats displayed a glioma in the neocortex surrounding the basal ganglia. The ratio of CPu to cortical damage (60:40) was identical in both WKY and SHR groups. Both the CPu (−36%) and the cortical volumes (−36%) of glioma were less in the SHR compared with that in the WKY rats.

Evolution of ADC within the tumor

ADC abnormalities, detected as hypersignals on the ADC maps, were notable from D11 and thereafter expanded (Figure 2a). ADC values in the contralateral hemisphere were similar in WKY and SHR and remained stable over time (Figure 2b). In both groups of rats, the tumors showed an increase in ADC values relative to the healthy tissue in the contralateral hemisphere (ANOVA—group effect: $P<0.01$; ROI effect: $P<0.0001$; interaction group × ROI: $P<0.07$) (Figure 2b). The increase in ADC values within the tumor compared with the healthy tissue was significant ($P<0.0001$) both in the SHR and WKY groups. Within the tumor, the ADC values were significantly different in the SHR group (with lower ADC values) compared with the WKY group ($P<0.02$), and for both groups, the ADC values increased in the tumor with time (ANOVA—group effect: $P<0.02$; time effect: $P<0.0001$; no interaction group × time: $P<0.4$) (Figure 2b). As a function of time, the minimum tumoral ADC values were lower in the SHR group compared with the WKY group (two-way ANOVA—group effect: $P=0.051$; time effect: $P=0.14$; time × group interaction: $P=0.14$) (Figure 2c). The mean of the minimum ADC values per group is lower in the SHR at D11 and D21 ($7.37E-04$; $7.46E-04$; $7.04E-04\ mm^2\ s^{-1}$ at D11, D18 and D21 after implantation) compared with the WKY group ($8.23E-04$; $7.36E-04$; $7.63E-04$-$mm^2\ s^{-1}$ at D11, D18 and D21 after implantation).

Evolution of hemodynamic parameters

In both groups, the first passage of Gd-DTPA was delayed within the tumor at D11 and D18 (Figure 3a). Quantitatively, in the healthy hemisphere, CBF and CBV values were not different between SHR and WKY (Figures 3b and c).

At D11, CBF and CBV values in the tumor were relatively similar to those measured in the contralateral hemisphere (ANOVA—group effect: 0.8; ROI effect: 0.6; interaction group × ROI: 0.2). At D18, the tumor in SHR displayed significant increases in CBF and CBV relative to the contralateral hemisphere (*t*-test, $P<0.0002$ for CBV; $P<0.0003$ for CBF following two-factor ANOVA with interaction group × ROI: $P<0.03$) (Figures 3b and c), whereas no significant effect was found in WKY rats. The comparison between hypertensive and normotensive rats showed that CBF and CBV were higher in the tumor in SHR at day 18 ($P<0.0085$ for CBV, $P<0.01$ for CBF).

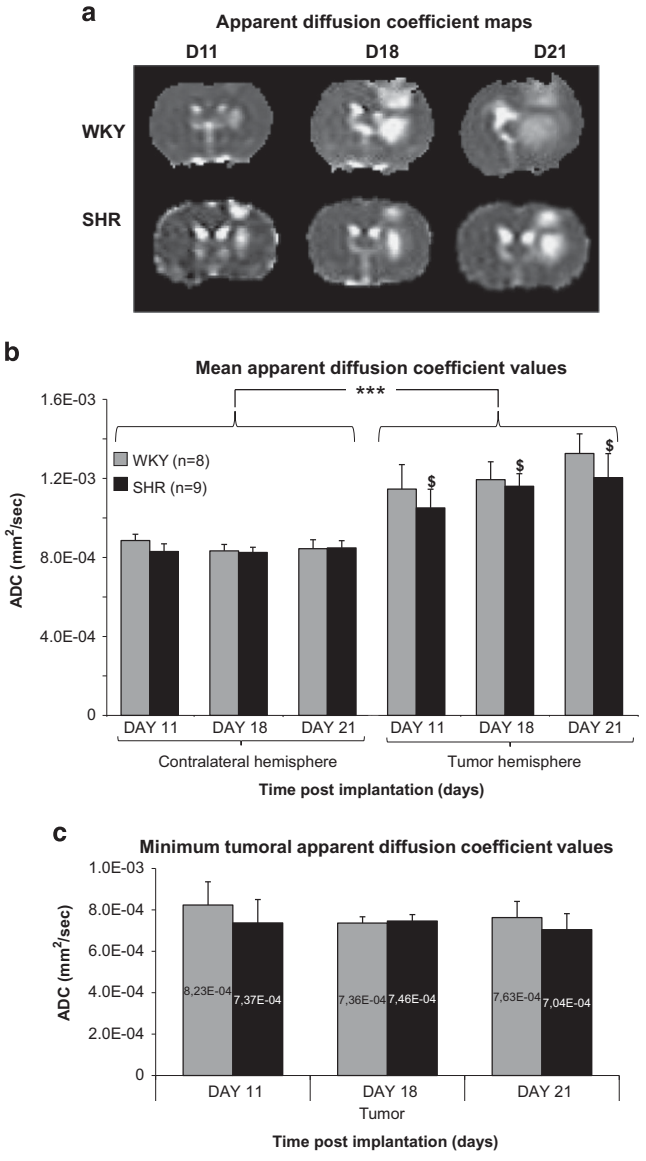

Figure 2 (**a**) Apparent diffusion coefficient (ADC) maps acquired at three post-implantation time points during the evolution of the tumor in representative Wistar–Kyoto (WKY) and spontaneously hypertensive rats (SHR). (**b**) Within the healthy non-implanted hemisphere, values of ADC in WKY rats and SHR were near identical at all the time points. ADC values were significantly greater in the tumor compared with the contralateral healthy tissue in SHR as well as in WKY rats (***$P<0.0001$; analysis of variance (ANOVA) main effect). ADC values were lesser in the tumor of SHR compared with the WKY ones ($^{\$}P<0.023$ ANOVA main effect). (**c**) The minimum ADC values within the tumor is four times lower in SHR compared with the WKY ones ($P=0.051$ ANOVA main effect).

Quantitative analysis of vessels in the tumor

In both hypertensive and normotensive rats, the vessels were clearly disorganized and their structure disturbed within the tumor compared with the healthy tissue in the contralateral hemisphere (Figure 4a). The vascular surface was significantly reduced in the center of the tumor, as well as in the periphery (Figure 4b) (two-way ANOVA with nonsignificant interaction followed by Tukey's HSD for ROI: $P<0.0001$). The vessels lengths were reduced in the tumor but not in the periphery (Figure 4c) (there was an ROI effect independent of the group analyzed; two-way ANOVA, significant group effect, significant ROI effect with nonsignificant interaction followed by Tukey's HSD for ROI: $P<0.0001$ (contralateral and periphery different from tumor, $P<0.0001$)).

Similarly, vessel diameters were increased in the tumor but not in the periphery relative to the contralateral hemisphere (two-way ANOVA, significant group effect, significant ROI effect with non-significant interaction followed by Tukey's HSD for ROI: $P<0.0001$ (contralateral and periphery different from tumor, $P<0.0001$)) (Figure 4d).

Quantitative histological analyses

The volume of the tumor, as assessed by volumetric histology, was less important in hypertensive compared with normotensive rats (ANOVA, $P<0.02$) (Figure 5a). The histological volumes were highly correlated to those defined on T2 images ($R^2=0.78$, $P<0.0001$, $n=17$). All the methodologies used showed a strong correlation in the evaluation of the differences in tumoral volumes between hypertensive and normotensive rats. As of note, the ratios in volume measured were: 0.73 assessed on T1-weighted imaging, 0.67 assessed on T2-weighted imaging, 0.75 on the growth coefficient slopes, 0.65 assessed on histology and 0.66 for the indices of hemispheric asymmetry. The volumetric assessment of the entire healthy hemisphere (healthy hemisphere volume: $393.05\pm43.48\,mm^3$ for WKY rats and $353.83\pm40.29\,mm^3$ for SHR) and the tumoral hemisphere (tumoral hemisphere volume: $488.51\pm61.15\,mm^3$ for WKY rats and $410.45\pm40.38\,mm^3$ for SHR) showed that the normotensive rats have a significantly expanded tumoral hemisphere compared with the contralateral healthy hemisphere ($P<0.0001$). Although there was no significant differences in the volume of the healthy hemispheres between SHR and WKY rats ($P>0.08$), WKY rats had a more volumetric tumoral hemisphere compared with hypertensive rats ($P<0.0107$).

Zones of necrosis were carefully delineated on thionin-stained slices and there were no major differences between groups. Necrosis was present in discrete foci within the tumoral mass and each focus was surrounded by pseudopalissadic cells. The necrotic portion of the tumor was on average $9.4\pm8.6\,mm^3$ for all the rats (the necrosis represented in percentage of the total tumoral volume: $12.1\pm9.9\%$ for SHR and $10.8\pm8.9\%$ for WKY). Necrosis was present in all the cortical tumors and represented 22% (in SHR) and 19% (in WKY rats) of the total volumes of pathology; the presence of necrotic tissue in the CPu was variable in both normo- and hypertensive strains and accounted for $<10\%$ of the total pathological volume. The fundamental, macroscopic features of the glioma were indistinguishable in both strains; the discriminatory factor was the rate of tumoral progression.

Inflammation

To examine if the different rates of tumoral expansion between WKY and SHR could be attributed to a differential inflammatory reaction in these two strains, we identified activated macrophages and microglia through the use of lectin histochemical staining (Figure 5b). All the rat brains presented lectin staining disseminated throughout the tumor, although the staining was more intense at the frontier between viable and tumoral tissue. Further, no observable difference in pattern and staining could be detected between the normotensive and hypertensive rats.

DISCUSSION

Here we demonstrate, for the first time, that CAH retards the growth of cerebral tumors. Brain tumors expanded more rapidly and were

more voluminous in normotensive compared with that in hypertensive rats as revealed by sequential MRI investigations and histology. Eleven days after cell implantation, both T1- and T2-weighted imaging demonstrated (at this early phase) that the volumes of the tumor were similar between normotensive and hypertensive animals. Given that the same number of cells was injected into the CPu, this lack of meaningful difference suggests that the initial process of tumor formation, which does not involve appreciable angiogenesis, was similar in the two groups of animals. Overall, MRI indices (volumetric measure of tumor from T1- and T2-weighted imaging, differential values of ADC and hemodynamic parameters, midline shift), as well as histological evaluation (tumor volume measurements and entire hemisphere volume), were all convergent. The dynamics of the glioma growth were accelerated in the normotensive rats. The slope coefficients of the tumor growth and the absence of significant differences between the intercepts attest to a decrease in the rate of tumor growth in hypertensive animals.

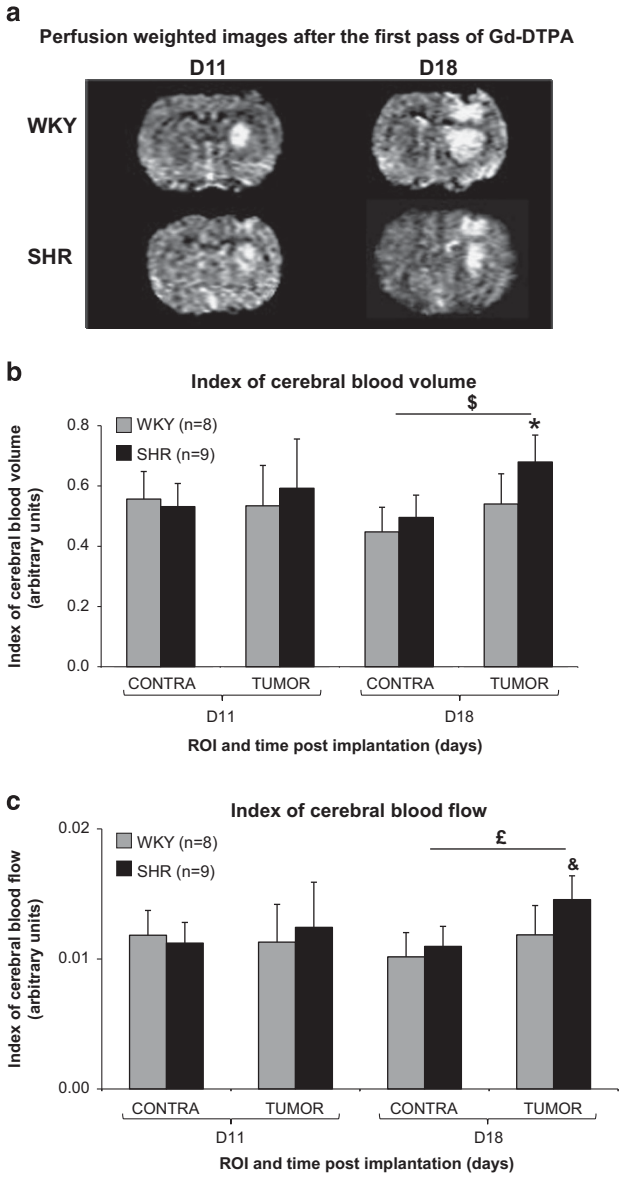

Figure 3 (**a**) Representative images of perfusion-weighted images showing, in both normotensive and hypertensive animals, a delayed passage of the Gd-DTPA (gadopentetate dimeglumine diethylenetriaminepentaacetic acid) within the tumor compared with the healthy tissue. (**b**) The evolution of an index of cerebral blood volume (CBV) in hypertensive and normotensive rats. CBV was derived from an algorithm based on the first pass of Gd-DTPA. At day 11 after implantation, there was no difference between spontaneously hypertensive (SHR) and Wistar–Kyoto (WKY) rats either in the contralateral hemisphere or in the tumor. However, at day 18 after implantation, SHR displayed an increased CBV in the tumor compared with the contralateral hemisphere (one-factor analysis of variance (ANOVA), $^{\$}P<0.00022$ for CBV; following ANOVA—group effect: 0.047; ROI effect: 0.0001; interaction group×ROI: 0.033). Thereafter, a one-factor ANOVA showed a group effect $P<0.0085$ (*) following a two-factor ANOVA, which demonstrated a significant group effect ($P<0.03$), ROI effect ($P<0.00001$) and significant interaction ($P<0.03$). (**c**) The evolution of an index of cerebral blood flow (CBF) in hypertensive and normotensive rats. As with CBV, CBF was derived from the first pass of Gd-DTPA. At day 11 after implantation, there was no difference between SHR and WKY in the contralateral hemisphere. Equally, there were no differences between the CBF circumscribed by the tumor in both rat strains. However, at day 18 after implantation, SHR had an increased CBF in the tumor compared with the contralateral hemisphere (ANOVA, one-factor, $^{£}P<0.00034$ for CBF following ANOVA—group effect: 0.047; ROI effect: 0.0001; interaction group×ROI: 0.033). In addition, a one-factor ANOVA showed a group effect $P<0.0152$ (&) following two-factor ANOVA showing significant group effect ($P<0.05$), ROI effect ($P<0.00001$) and significant interaction ($P<0.04$).

SHR and WKY rats share the same genetic background, and as shown, the[36,37] inflammatory reactions were similar between the two strains,[38] which might exclude the influence of these processes. Specifically, the distribution and numbers of the histochemical evaluation of microglia and macrophages was undertaken to rule out this possibility. The difference observed in tumor volumes between hypertensive and normotensive animals is unlikely to be attributed to rejection or inflammatory reactions.

The tumor in hypertensive animals displayed a significantly lower ADC compared with normotensive animals. This difference may result from variations in cell density or vasogenic edema between the two strains.[39] Some consider that minimal ADC values can help in the identification of patients with a favorable prognosis.[40] While accepting an ongoing debate as to its pertinence, minimum ADC is more and more used in clinical studies to evaluate its potential as a biomarker of prognosis. According to the literature, lower minimum ADC is related to poor prognosis in the absence of treatment,[41] but it has been recently shown that low minimum ADC values could constitute a biomarker of favorable response to treatment.[41–43] Those patients treated with an antiangiogenic regimen had the lowest minimum ADC values and showed a more favorable prognosis compared with patients with greater minimum ADC.[41–43] A lower minimum ADC in SHR compared with WKY animals is consistent with these clinical observations. Our observations support a more favorable outcome of tumors presenting with lower minimum ADC and lower ADC values, namely here, tumors grown under hypertensive conditions.

As CAH markedly affects the vasculature and particularly angiogenesis[21] (both are of major importance to the growth of the tumor),[44] we advance the hypothesis that the slow growth of the glioma (in the presence of essential hypertension) can be attributed to hypertension-induced effects on the cerebrovascular system. As shown by the vessel morphology analysis, in the center of the tumor, the vessel's surface and the vessel's length were reduced but the vessels' diameter was increased in comparison with the healthy tissue. The

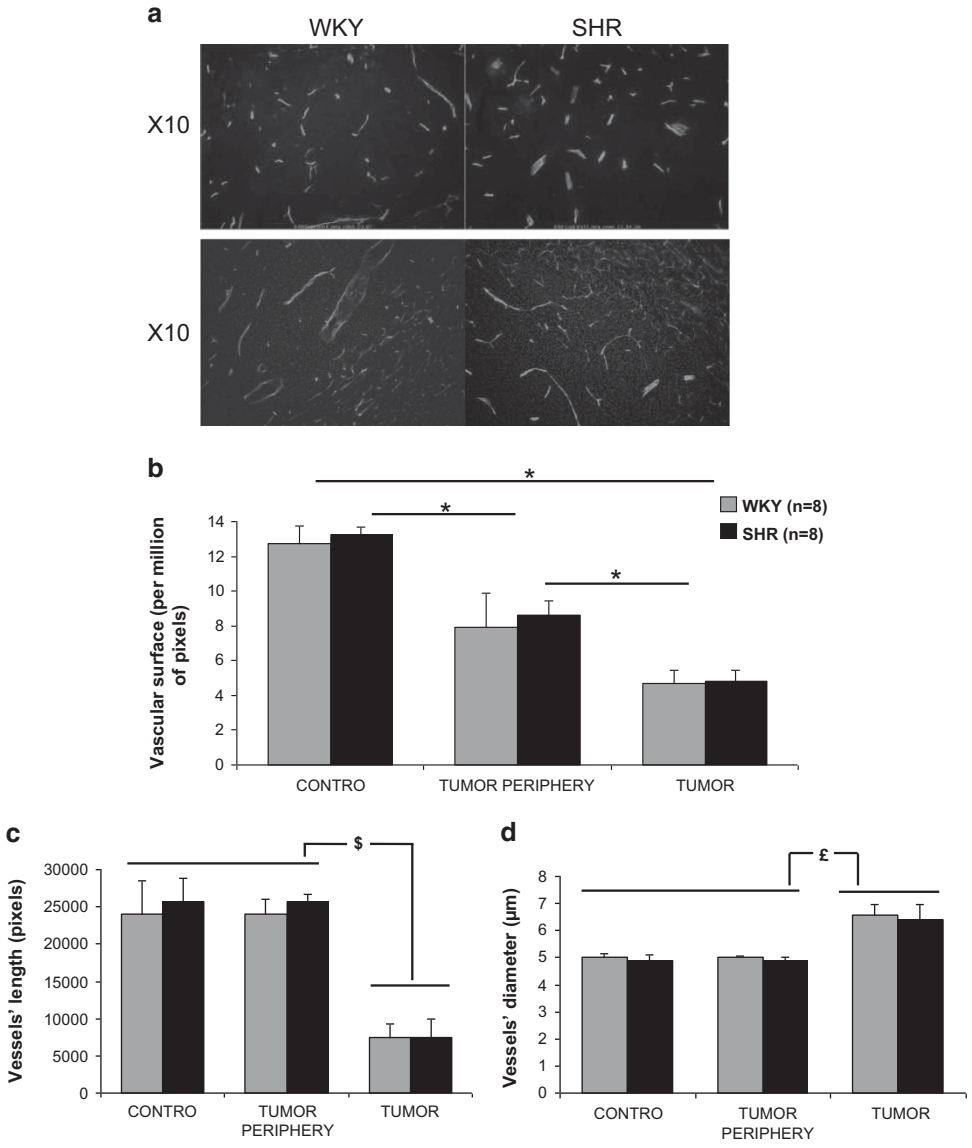

Figure 4 (**a**) Illustration of the core of the tumor and the tumor periphery visualized after immunological staining for cells nuclei and blood vessels (red color: endothelial cells immunolabelled with RECA antibody, x10; blue color: nucleus cells counterstained with Hoescht 33342, x10). (**b**) Morphological analysis of vessels: regarding the vascular surface, there was no difference between groups. There was a significant difference, independent of the group considered, between each ROI, with a progressive decrease of the vascular surface from the contralateral healthy tissue to the periphery of the tumor to the tumor. $^{*}P<0.0001$. (**c**) The vessels length were reduced in the tumor compared with the periphery and the contralateral hemisphere. $^{\$}P<0.0001$, Tukey's HSD following two-factor analysis of variance (ANOVA). (**d**) The vessel diameters were also increased in the tumor compared with the periphery and the contralateral hemisphere ($^{£}P<0.0001$ Tukey's HSD). A full color version of this figure is available at the *Hypertension Research* journal online.

periphery of the tumor was almost comparable regarding the structure of vessels to the contralateral but was significantly different from the tumor and contralateral regarding the vascular surface. Neither the structure nor the organization of the vessels displayed differences between SHR and WKY rats both in the periphery and the center of the tumor. Although we did not see any difference in structural or density of vessels in the tumor between SHR and WKY rats, this does not mean that angiogenesis was similar between the two conditions. Less efficient angiogenesis at earlier stages may have slowed down the proliferation of the tumor. Indeed, in our experimental setting, histological studies were performed at an advanced stage at which tumors become less hypoxic and angiogenesis may be less involved than at earlier stage in which the amplitude of hypoxia is greater.[26] In this case, angiogenesis in hypertensive animals may be longer to be settled compared with that in normotensive ones. The installation of angiogenesis in hypertensive animals may take longer compared with that in normotensive rats.

Alternatively, the phenomenon of angiogenesis might be impaired compared with normotensive rats.

Antiangiogenic therapies induce hypertension as a side effect. It has been reported in the literature that treatment-induced hypertension might be a positive prognostic criterion. For example, pancreatic cancer studies have reported a longer survival for patients with sunitinib- or bevacizumab-related hypertension.[45–47] In renal carcinoma, similar outcomes have been observed with axitinib treatment.[46] Others were unable to confirm a prognostic value of elevated AP for

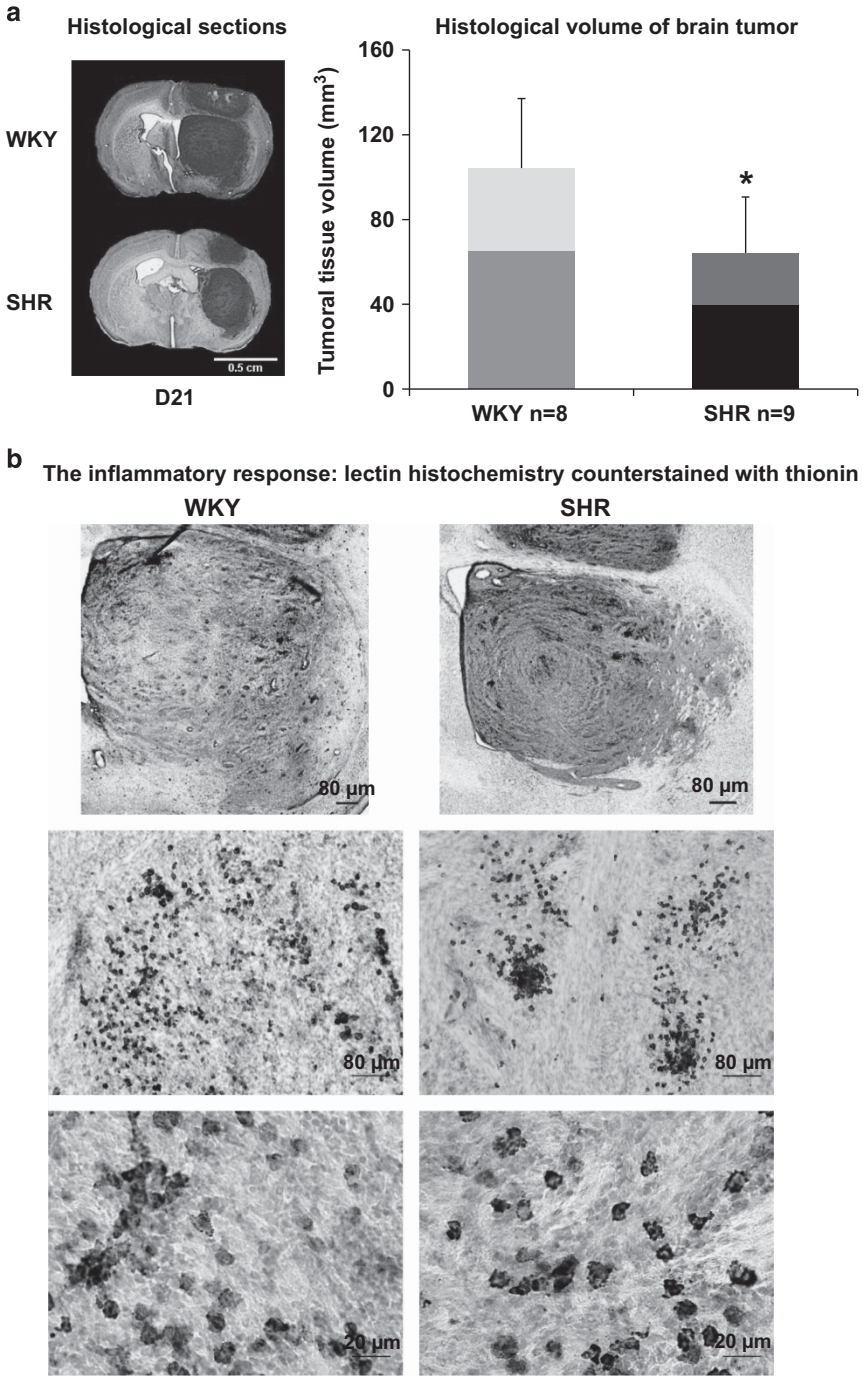

Figure 5 (**a**) Post-mortem analysis: histological tumor volume quantification. Representative histological sections stained within thionin, performed at day 21. Histograms represent the striatal part of the tumor (dark gray for Wistar–Kyoto (WKY) and black for spontaneously hypertensive (SHR)) and the cortical part of the tumor (light gray for WKY and dark gray for SHR). The post-mortem analysis confirmed that the tumor was significantly more important in WKY compared with that in SHR (one-factor analysis of variance (ANOVA), $*P<0.02$). (**b**) Post-mortem analysis: inflammatory response. Illustration of lectin histochemistry counterstained with thionin. Activated microglia are seen as small round brown cells and were observed only in the tumoral region and never seen in the contralateral hemispheres of both WKY and SHR. The features of the glial reactions were similar in the two groups. The boxes indicate the different magnifications of the illustration. A full color version of this figure is available at the *Hypertension Research* journal online.

GBM, but the investigation had a small cohort including a few patients with treatment-induced hypertension.[48] Conversely, Lombardi *et al.*[49] found hypertension to be an effective biomarker in patients suffering from recurrent GBM treated with antiangiogenic agents. Hypertension in those patients was associated with an improved overall survival. In summary, the data in the literature strongly suggest an impact of hypertension on tumor development as well as on a potential beneficial outcome.

If cancer treatment-induced hypertension seems to be indicative of a less severe prognosis, there is as of now no consensus regarding the

management of the induced hypertension, except the fact that blood pressure has to be monitored and maintained within acceptable limits to finish the antiangiogenic treatment.[50–52] The impact of the different categories of antihypertensive drugs on the cancer evolution and prognosis has not been investigated.[53] The antihypertensive drugs are numerous and there are not enough data available in the different combinations of cancer, cancer evolution, cancer treatment and antihypertensive drug class to enable the publication of guidelines. For long, antihypertensive drugs have been considered to be a carcinogen, but there is not enough evidence in the literature to obtain a coherent view or consensus and there are some data to indicate that antihypertensive drugs could even be beneficial.[54] For example, angiotensin-converting enzyme inhibitors could have anti-GBM activity.[55] Although hypertensive drugs might represent a risk factor for breast cancer,[56] they can also slow cancer progression in other cases. For example, β-blockers have a positive impact on melanoma and novel angiotensin II AT1 receptor antagonist could have antitumor activity in prostate cancer.[57,58] In general, β-blockers are associated with longer survival in different types of cancer.[59,60] Thus, certain antihypertensive drugs might possess an antitumor activity. These varied references illustrate that the intrication of cancer and hypertension is highly complicated. Yet, even further, the relations between cancer and antihypertensive drugs might be a function of the type of antihypertensive drug, the type of cancer, the tumor phenotype and finally the cancer treatment. Complete prospective studies are needed to analyze the impact of antihypertensive drugs in cancer evolution and prognosis.[61] In such studies, it appears important to know if antihypertensive drugs would obtund or not the hypertension-related beneficial prognosis observed and if all hypertensive drugs would have the same effect on this hypertension-related prognosis in glioma patients.

In addition, the vessels potentially present a higher altered functionality within the tumor of hypertensive animals. Indeed, it is well known that CAH affects different features of the physiology and pathophysiology of the cerebrovasculature.[15,62,63] These modifications could impede the invasion of the tumor in the neuropil. In terms of the hemodynamic parameters we assessed, our data have shown an increased CBF and CBV in the tumor that was more marked in SHR compared with WKY, whereas the two groups displayed similar values in the contralateral healthy tissue. These data are in agreement with those from the literature that report an increased relative CBV and CBF within the tumor.[64] Furthermore, it has been recently shown that C6 glioma (treated with a disulfonyl derivative of phenyl-*tert*-butyl nitrone, a molecule that displays antiglioma activity and results in a reduced tumor size) have an increased perfusion rate compared with untreated tumors.[65] More recently, Sorensen *et al*.[66] showed that, in a population of patients treated with cediranib, those with a sustained increased tumor perfusion had a longer survival. Their study underlines the ability of an antiangiogenic therapy to increase perfusion in the tumor and so to improve patient outcome.[66]

CONCLUSIONS

The results of this study put into light, for the first time, the influence of a frequent and highly deleterious pathology, CAH, on the evolution of the most frequent adult brain tumor, the GBM. Chronic hypertension significantly slows down glioma growth. A better understanding of the interaction of those two complex pathologies seems a necessity to improve patient care and potential treatment success.

CONFLICT OF INTEREST

The authors declare no conflict of interest.

ACKNOWLEDGEMENTS

This study was supported by the Centre National de la Recherche Scientifique (CNRS), the Conseil Régional de Basse-Normandie and the Université de Caen Basse-Normandie.

1 Clarke J, Butowski N, Chang S. Recent advances in therapy for glioblastoma. *Arch Neurol* 2010; **67**: 279–283.
2 Nishikawa R. Standard therapy for glioblastoma—a review of where we are. *Neurol Med Chir (Tokyo)* 2010; **50**: 713–719.
3 Jain RK, di Tomaso E, Duda DG, Loeffler JS, Sorensen AG, Batchelor TT. Angiogenesis in brain tumours. *Nat Rev Neurosci* 2007; **8**: 610–622.
4 Miletic H, Niclou SP, Johansson M, Bjerkvig R. Anti-VEGF therapies for malignant glioma: treatment effects and escape mechanisms. *Expert Opin Ther Targets* 2009; **13**: 455–468.
5 Bertolini F, Marighetti P, Martin-Padura I, Mancuso P, Hu-Lowe DD, Shaked Y, D'Onofrio A. Anti-VEGF and beyond: shaping a new generation of anti-angiogenic therapies for cancer. *Drug Discov Today* 2011; **16**: 1052–1060.
6 Shirai K, Siedow MR, Chakravarti A. Antiangiogenic therapy for patients with recurrent and newly diagnosed malignant gliomas. *J Oncol* 2012; **2012**: 193436.
7 Kearney PM, Whelton M, Reynolds K, Muntner P, Whelton PK, He J. Global burden of hypertension: analysis of worldwide data. *Lancet* 2005; **365**: 217–223.
8 Chobanian AV. Shattuck Lecture. The hypertension paradox—more uncontrolled disease despite improved therapy. *N Engl J Med* 2009; **361**: 878–887.
9 López-Jaramillo P, Velandia-Carrillo C, Alvarez-Camacho J, Cohen DD, Sánchez-Solano T, Castillo-López G. Inflammation and hypertension: are there regional differences? *Int J Hypertens* 2013; **2013**: 492094.
10 Arnold AC, Gallagher PE, Diz DI. Brain renin–angiotensin system in the nexus of hypertension and aging. *Hypertens Res* 2013; **36**: 5–13.
11 Yagi S, Akaike M, Ise T, Ueda Y, Iwase T, Sata M. Renin–angiotensin–aldosterone system has a pivotal role in cognitive impairment. *Hypertens Res* 2013; **36**: 753–758.
12 Lawes CMM, Vander Hoorn S, Rodgers A. Global burden of blood-pressure-related disease, 2001. *Lancet* 2008; **371**: 1513–1518.
13 Schiffrin EL. Remodeling of resistance arteries in essential hypertension and effects of antihypertensive treatment. *Am J Hypertens* 2004; **17**: 1192–1200.
14 Spieker LE, Flammer AJ, Lüscher TF. The vascular endothelium in hypertension. *Handb Exp Pharmacol* 2006;: 249–283.
15 Paulson OB, Strandgaard S, Edvinsson L. Cerebral autoregulation. *Cerebrovasc Brain Metab Rev* 1990; **2**: 161–192.
16 Fujishima M, Ibayashi S, Fujii K, Mori S. Cerebral blood flow and brain function in hypertension. *Hypertens Res* 1995; **18**: 111–117.
17 Valenzuela M, Esler M, Ritchie K, Brodaty H. Antihypertensives for combating dementia? A perspective on candidate molecular mechanisms and population-based prevention. *Transl Psychiatry* 2012; **2**: e107.
18 Waki H, Gouraud SS, Maeda M, Raizada MK, Paton JFR. Contributions of vascular inflammation in the brainstem for neurogenic hypertension. *Respir Physiol Neurobiol* 2011; **178**: 422–428.
19 Pires PW, Dams Ramos CM, Matin N, Dorrance AM. The effects of hypertension on the cerebral circulation. *Am J Physiol Heart Circ Physiol* 2013; **304**: H1598–H1614.
20 Emanueli C, Salis MB, Stacca T, Gaspa L, Chao J, Chao L, Piana A, Madeddu P. Rescue of impaired angiogenesis in spontaneously hypertensive rats by intramuscular human tissue kallikrein gene transfer. *Hypertension* 2001; **38**: 136–141.
21 Feihl F, Liaudet L, Waeber B, Levy BI. Hypertension: a disease of the microcirculation? *Hypertension* 2006; **48**: 1012–1017.
22 Simonsen U, Aalkjaer C. Small artery structure and function: a dual interaction with many players. *Basic Clin Pharmacol Toxicol* 2012; **110**: 2–4.
23 Sullivan JM, Prewitt RL, Josephs JA. Attenuation of the microcirculation in young patients with high-output borderline hypertension. *Hypertension* 1983; **5**: 844–851.
24 Takeshita S, Tomiyama H, Yokoyama N, Kawamura Y, Furukawa T, Ishigai Y, Shibano T, Isshiki T, Sato T. Angiotensin-converting enzyme inhibition improves defective angiogenesis in the ischemic limb of spontaneously hypertensive rats. *Cardiovasc Res* 2001; **52**: 314–320.
25 Lerman LO, Chade AR, Sica V, Napoli C. Animal models of hypertension: an overview. *J Lab Clin Med* 2005; **146**: 160–173.
26 Valable S, Petit E, Roussel S, Marteau L, Toutain J, Divoux D, Sobrio F, Delamare J, Barré L, Bernaudin M. Complementary information from magnetic resonance imaging and (18)F-fluoromisonidazole positron emission tomography in the assessment of the response to an antiangiogenic treatment in a rat brain tumor model. *Nucl Med Biol* 2011; **38**: 781–793.
27 Barth RF, Kaur B. Rat brain tumor models in experimental neuro-oncology: the C6, 9 L, T9, RG2, F98, BT4C, RT-2 and CNS-1 gliomas. *J Neurooncol* 2009; **94**: 299–312.
28 Sibenaller ZA, Etame AB, Ali MM, Barua M, Braun TA, Casavant TL, Ryken TC. Genetic characterization of commonly used glioma cell lines in the rat animal model system. *Neurosurg Focus* 2005; **19**: E1.
29 Letourneur A, Roussel S, Toutain J, Bernaudin M, Touzani O. Impact of genetic and renovascular chronic arterial hypertension on the acute spatiotemporal evolution of the ischemic penumbra: a sequential study with MRI in the rat. *J Cereb Blood Flow Metab* 2011; **31**: 504–513.

30 Valable S, Barbier EL, Bernaudin M, Roussel S, Segebarth C, Petit E, Rémy C. *In vivo* MRI tracking of exogenous monocytes/macrophages targeting brain tumors in a rat model of glioma. *NeuroImage* 2008; **40**: 973–983.
31 Paxinos G, Watson C. *The Rat Brain in Stereotaxic Coordinates: Hard Cover Edition*. Academic Press: New York, NY, USA.
32 Rasband WS. *ImageJ*. U. S. National Institutes of Health, Bethesda, MD, USA, http://imagej.nih.gov/ij/, 1997–2014.
33 Schneider CA, Rasband WS, Eliceiri KW. NIH Image to ImageJ: 25 years of image analysis. *Nat Methods* 2012; **9**: 671–675.
34 Blasberg RG, Kobayashi T, Horowitz M, Rice JM, Groothuis D, Molnar P, Fenstermacher JD. Regional blood flow in ethylnitrosourea-induced brain tumors. *Ann Neurol* 1983; **14**: 189–201.
35 Valable S, Eddi D, Constans J-M, Guillamo J-S, Bernaudin M, Roussel S, Petit E. MRI assessment of hemodynamic effects of angiopoietin-2 overexpression in a brain tumor model. *Neuro-oncology* 2009; **11**: 488–502.
36 Okamoto K, Aoki K. Development of a strain of spontaneously hypertensive rats. *Jpn Circ J* 1963; **27**: 282–293.
37 Okamoto K, Tabei R, Fukushima M, Nosaka S, Yamori Y, Ichijima K, Haebara H, Matsumoto M, Maruyama T, Suzuki Y, Tamegai M. Further observations of the development of a strain of spontaneously hypertensive rats. *Jpn Circ J* 1966; **30**: 703–716.
38 Gonzalez-Martin A, Muñoz-Espin D, Alonso AM, Izquierdo M. Parent phenotype and age dependence, on rat glioma tumor rejection. *J Neurooncol* 2004; **70**: 29–34.
39 Valable S, Lemasson B, Farion R, Beaumont M, Segebarth C, Remy C, Barbier EL. Assessment of blood volume, vessel size, and the expression of angiogenic factors in two rat glioma models: a longitudinal *in vivo* and *ex vivo* study. *NMR Biomed* 2008; **21**: 1043–1056.
40 Higano S, Yun X, Kumabe T, Watanabe M, Mugikura S, Umetsu A, Sato A, Yamada T, Takahashi S. Malignant astrocytic tumors: clinical importance of apparent diffusion coefficient in prediction of grade and prognosis. *Radiology* 2006; **241**: 839–846.
41 Romano A, Calabria LF, Tavanti F, Minniti G, Rossi-Espagnet MC, Coppola V, Pugliese S, Guida D, Francione G, Colonnese C, Fantozzi LM, Bozzao A. Apparent diffusion coefficient obtained by magnetic resonance imaging as a prognostic marker in glioblastomas: correlation with MGMT promoter methylation status. *Eur Radiol* 2013; **23**: 513–520.
42 Nagane M, Kobayashi K, Tanaka M, Tsuchiya K, Shishido-Hara Y, Shimizu S, Shiokawa Y. Predictive significance of mean apparent diffusion coefficient value for responsiveness of temozolomide-refractory malignant glioma to bevacizumab: preliminary report. *Int J Clin Oncol* 2014; **19**: 16–23.
43 Sunwoo L, Choi SH, Park C-K, Kim JW, Yi KS, Lee WJ, Yoon TJ, Song SW, Kim JE, Kim JY, Kim TM, Lee S-H, Kim J-H, Sohn C-H, Park S-H, Kim IH, Chang K-H. Correlation of apparent diffusion coefficient values measured by diffusion MRI and MGMT promoter methylation semiquantitatively analyzed with MS-MLPA in patients with glioblastoma multiforme. *J Magn Reson Imag* 2013; **37**: 351–358.
44 Wong MLH, Prawira A, Kaye AH, Hovens CM. Tumour angiogenesis: its mechanism and therapeutic implications in malignant gliomas. *J Clin Neurosci* 2009; **16**: 1119–1130.
45 Bono P, Elfving H, Utriainen T, Osterlund P, Saarto T, Alanko T, Joensuu H. Hypertension and clinical benefit of bevacizumab in the treatment of advanced renal cell carcinoma. *Ann Oncol* 2009; **20**: 393–394.
46 Escudier B, Gore M. Axitinib for the management of metastatic renal cell carcinoma. *Drugs R D* 2011; **11**: 113–126.
47 Rixe O, Billemont B, Izzedine H. Hypertension as a predictive factor of Sunitinib activity. *Ann Oncol* 2007; **18**: 1117.
48 Wick A, Schäfer N, Dörner N, Schemmer D, Platten M, Bendszus M, Wick W. Arterial hypertension and bevacizumab treatment in glioblastoma: no correlation with clinical outcome. *J Neuro-Oncol* 2009; **97**: 157–158.
49 Lombardi G, Zustovich F, Farina P, Fiduccia P, Della Puppa A, Polo V, Bertorelle R, Gardiman MP, Banzato A, Ciccarino P, Denaro L, Zagonel V. Hypertension as a biomarker in patients with recurrent glioblastoma treated with antiangiogenic drugs: a single-center experience and a critical review of the literature. *Anticancer Drugs* 2013; **24**: 90–97.
50 Bamias A, Manios E, Karadimou A, Michas F, Lainakis G, Constantinidis C, Deliveliotis C, Zakopoulos N, Dimopoulos MA. The use of 24-h ambulatory blood pressure monitoring (ABPM) during the first cycle of sunitinib improves the diagnostic accuracy and management of hypertension in patients with advanced renal cancer. *Eur J Cancer* 2011; **47**: 1660–1668.
51 Ferroni P, Della-Morte D, Palmirotta R, Rundek T, Guadagni F, Roselli M. Angiogenesis and hypertension: the dual role of anti-hypertensive and anti-angiogenic therapies. *Curr Vasc Pharmacol* 2012; **10**: 479–493.
52 Wook Shin D, Young Kim S, Cho J, Kook Yang H, Cho B, Nam H-S, Kim H, Park J-H. Comparison of hypertension management between cancer survivors and the general public. *Hypertens Res* 2012; **35**: 935–939.
53 De Jesus-Gonzalez N, Robinson E, Moslehi J, Humphreys BD. Management of antiangiogenic therapy-induced hypertension. *Hypertension* 2012; **60**: 607–615.
54 Singh A, Bangalore S. Which, if any, antihypertensive agents cause cancer? *Curr Opin Cardiol* 2012; **27**: 374–380.
55 Kast RE, Halatsch M-E. Matrix metalloproteinase-2 and -9 in glioblastoma: a trio of old drugs-captopril, disulfiram and nelfinavir-are inhibitors with potential as adjunctive treatments in glioblastoma. *Arch Med Res* 2012; **43**: 243–247.
56 Li CI, Daling JR, Tang M-TC, Haugen KL, Porter PL, Malone KE. Use of antihypertensive medications and breast cancer risk among women aged 55 to 74 years. *JAMA Intern Med* 2013; **173**: 1629–1637.
57 Da Y, Yuan W, Xin T, Nie Y, Ye Y, Yan Y-J, Liang L, Chen Z. Synthesis and biological evaluation of new fluorine substituted derivatives as angiotensin II receptor antagonists with anti-hypertension and anti-tumor effects. *Bioorg Med Chem* 2012; **20**: 7101–7111.
58 De Giorgi V, Gandini S, Grazzini M, Benemei S, Marchionni N, Geppetti P. Effect of β-blockers and other antihypertensive drugs on the risk of melanoma recurrence and death. *Mayo Clin Proc* 2013; **88**: 1196–1203.
59 Diaz ES, Karlan BY, Li AJ. Impact of beta blockers on epithelial ovarian cancer survival. *Gynecol Oncol* 2012; **127**: 375–378.
60 Jansen L, Hoffmeister M, Arndt V, Chang-Claude J, Brenner H. Stage-specific associations between beta blocker use and prognosis after colorectal cancer. *Cancer* 2014; **120**: 1178–1186.
61 Milan A, Puglisi E, Ferrari L, Bruno G, Losano I, Veglio F. Arterial hypertension and cancer. *Int J Cancer* 2014; **134**: 2269–2277.
62 Baumbach GL. Effects of increased pulse pressure on cerebral arterioles. *Hypertension* 1996; **27**: 159–167.
63 Iadecola C, Davisson RL. Hypertension and cerebrovascular dysfunction. *Cell Metab* 2008; **7**: 476–484.
64 Ulmer S, Liess C, Kesari S, Otto N, Straube T, Jansen O. Use of dynamic susceptibility-contrast MRI (DSC-MRI) to assess perfusion changes in the ipsilateral brain parenchyma from glioblastoma. *J Neurooncol* 2009; **91**: 213–220.
65 Garteiser P, Doblas S, Watanabe Y, Saunders D, Hoyle J, Lerner M, He T, Floyd RA, Towner RA. Multiparametric assessment of the anti-glioma properties of OKN007 by magnetic resonance imaging. *J Magn Reson Imag* 2010; **31**: 796–806.
66 Sorensen AG, Emblem KE, Polaskova P, Jennings D, Kim H, Ancukiewicz M, Wang M, Wen PY, Ivy P, Batchelor TT, Jain RK. Increased survival of glioblastoma patients who respond to antiangiogenic therapy with elevated blood perfusion. *Cancer Res* 2012; **72**: 402–407.

Supplementary Information accompanies the paper on Hypertension Research website (http://www.nature.com/hr)